Galaxy-cluster masses via 21st-century measurements of lensing of 21-cm fluctuations

Ely D. Kovetz and Marc Kamionkowski

Phys. Rev. D **87**, 063516 — Published 14 March 2013

DOI: 10.1103/PhysRevD.87.063516

Galaxy-Cluster Masses via 21st-Century Measurements of Lensing of 21-cm Fluctuations

Ely D. Kovetz[1] and Marc Kamionkowski[2]
[1] *Theory Group, Department of Physics and Texas Cosmology Center, The University of Texas at Austin, TX 78712, USA and*
[2] *Department of Physics and Astronomy, Johns Hopkins University, Baltimore, MD 21218, USA*

We discuss the prospects to measure galaxy-cluster properties via weak lensing of 21-cm fluctuations from the dark ages and the epoch of reionization (EoR). We choose as a figure of merit the smallest cluster mass detectable through such measurements. We construct the minimum-variance quadratic estimator for the cluster mass based on lensing of 21-cm fluctuations at multiple redshifts. We discuss the tradeoff between frequency bandwidth, angular resolution, and number of redshift shells available for a fixed noise level for the radio detectors. Observations of lensing of the 21-cm background from the dark ages will be capable of detecting $M \gtrsim 10^{12}\,h^{-1}M_\odot$ mass halos, but will require futuristic experiments to overcome the contaminating sources. Next-generation radio measurements of 21-cm fluctuations from the EoR will, however, have the sensitivity to detect galaxy clusters with halo masses $M \gtrsim 10^{13}\,h^{-1}M_\odot$, given enough observation time (for the relevant sky patch) and collecting area to maximize their resolution capabilities.

I. INTRODUCTION

The hyperfine transition of neutral hydrogen at 21 cm provides a unique source of cosmological information from the epoch of reionization (EoR) and the dark ages [1, 2]. It is the target of several ongoing and near-future ground-based experiments [3], as well as more distant prospects such as a Lunar-based observatory [4]. During the two relevant cosmological epochs, the dark ages and the EoR, the hyperfine transition is observed in absorption or emission, respectively, against the cosmic microwave background (CMB). By measuring this signal at different frequencies, the large redshift volume of these two epochs can be used to generate independent images of the spatial distribution of neutral hydrogen at different redshifts [5–7].

The image of the 21-cm signal from the dark ages and/or EoR should appear on the sky as a random field described by some statistically isotropic two-point correlation function. If, however, that image is distorted by weak gravitational lensing from foreground matter—either the large-scale inhomogeneous distribution of mass in the Universe or by discrete objects, like galaxy clusters—then there may be local departures from statistical isotropy induced [8–14]. Measurement of these local departures from statistical isotropy may thus allow a measurement of the distribution of this intervening matter.

The effects of gravitational lensing of 21-cm anisotropies are the same as the analogous effects on CMB fluctuations and can therefore be analyzed with the tools developed for lensing of the CMB [15–17]. However, the extension of 21-cm fluctuations to far smaller angular scales (limited in principle only by the baryonic Jeans mass [6]) than CMB fluctuations (which are suppressed on small scales by Silk damping [18]), as well as the possibility to see images of the 21-cm background at multiple redshifts, make 21-cm lensing far more promising, ultimately, for weak-lensing studies. In particular, constraining the parameters of galaxy cluster mass profiles using weak lensing reconstruction can be a useful tool in probing the evolution of dark energy [19] and studying the properties of dark matter (e.g. through the characterization of substructure or the mapping of its distribution in merging clusters).

High-resolution imaging of the mass distribution in galaxy clusters using 21-cm lensing was investigated in Ref. [10] (and with simulations in Ref. [11]). This work concluded that while forthcoming experiments may have the potential to provide some initial detections of galaxy clusters, the full promise of the technique will likely have to await subsequent generations.

The goal of this paper is to re-visit lensing of the 21-cm background by galaxy clusters with an analytic treatment aimed primarily to help understand the dependence of the detectability of the signal on experimental parameters. The aim will be to clarify the experimental requirements for such detections and to assist in the design of experiments to make such measurements. More specifically, we use as a figure of merit the smallest galaxy-cluster mass detectable by a given experimental configuration and then investigate the dependence of this threshold mass on the experimental configuration.

The plan of the paper is as follows: In Section II, we review the 21-cm signal and examine its dependence on the observation frequency and on the bandwidth over which the signal is observed. In Section III we discuss the noise power spectrum of radio interferometers and study its dependence on frequency, bandwidth, angular resolution, observation time, and collecting area. In Section IV we review how lensing of the 21-cm background by galaxy-cluster masses is accomplished. We present a quadratic estimator for the weak-lensing convergence and derive the noise with which it can be measured. In Section V we construct a minimum-variance estimator for the galaxy-cluster mass obtained from the lensing convergence and derive a formula for the smallest detectable

galaxy-cluster mass as a function of the various experimental parameters, assuming an NFW mass profile. In Section VI we show the results for galaxy-cluster mass detectability with next generation interferometers as well as futuristic ideal experiments and discuss different tradeoffs between the experimental parameters. In Section VII we compare the prospects for mass measurements from lensing of 21-cm fluctuations with other mass measurements, mention possible improvements to our estimator and discuss some relevant subtleties. We conclude in Section VIII.

II. 21-CM EMISSION/ABSORPTION SIGNAL

We begin by reviewing the physics responsible for producing the 21-cm signal from the dark ages and the EoR, whose relative comoving volumes are illustrated in Fig. 1. Defining the spin temperature T_s as the excitation temperature of the hyperfine transition (characterizing the ratio between the number densities of hydrogen atoms in the excited and ground-state levels), the rest-frame brightness temperature of a patch of the sky is given by $T_b = T_{\rm CMB}e^{-\tau} + T_S(1-e^{-\tau})$, where the optical depth for the hyperfine transition is [20]

$$\tau \;=\; \frac{3c^3\hbar A_{10}\, n_{\rm HI}}{16k\nu_0^2\, T_S\, H(z)}, \qquad (1)$$

$A_{10} = 2.85\times10^{-15}\,{\rm s}^{-1}$ is the Einstein coefficient for the transition, $\nu_0 = 1420\,{\rm MHz}$ its rest-frame frequency and $n_{\rm HI}$ is the local neutral hydrogen density. The brightness temperature in this patch, at an observed frequency ν corresponding to a redshift $1+z=\nu_0/\nu$, and the CMB is given by the difference

$$\delta T_b(\nu) \;\approx\; \frac{T_S - T_{\rm CMB}}{1+z}\,\tau. \qquad (2)$$

Hence if the excitation temperature T_s in a region differs from that of the CMB, the region will appear in emission (if $T_s > T_{\rm CMB}$) or absorption (if $T_s < T_{\rm CMB}$) against the CMB.

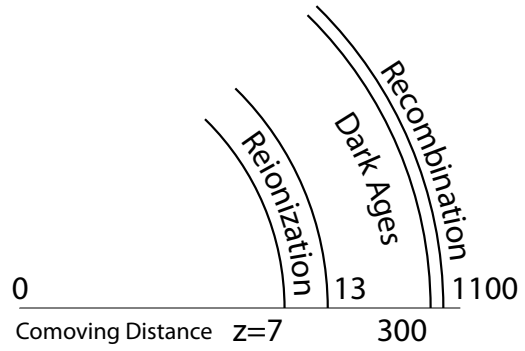

FIG. 1: An illustration of the comoving volume of the universe demonstrating the huge potential for extracting valuable information from 21-cm radiation in the dark ages and the reionization epochs.

During the dark ages, there is a redshift period $30 < z < 200$ where neutral hydrogen should be visible in absorption against the CMB, as the spin temperature is coupled to the gas temperature (and cools adiabatically as $(1+z)^2$) while collisions are efficient and drops below the CMB temperature (which only cools as $(1+z)$), a process that peaks at $z\sim70$ and lasts until the Hubble expansion renders collisions inefficient and $T_s \sim T_{\rm CMB}$ again at $z\sim30$. The signal from this early epoch is not affected by nonlinear density structures nor contaminated by astrophysical sources, which have yet to form.

A 21-cm signal is also accessible during the EoR, at redshifts $7 \lesssim z \lesssim 13$, when newly formed structure heated up neutral hydrogen but before the hydrogen became fully ionized. Predicting the brightness-temperature signal in this epoch is much harder, as astrophysical noise sources are substantial and our uncertainties as to the beginning and duration of this period are significant. Unlike the dark ages signal, in order to plot the signal during reionization we need to trace the redshift behavior of the neutral gas fraction which determines the optical depth, Eq. (1), for the hyperfine transition.

In Appendix A, we review the power spectrum of intensity fluctuations of 21-cm radiation. Eqs. (A3)-(A5) describe the angular power spectrum and its approximated form in the limit of large and small scales. In observations of these fluctuations, an important factor is the damping that results from line-of-sight averaging in a width δr (corresponding to an observed bandwidth $\Delta\nu$) around the distance r to the desired frequency ν, whose scale is determined for a given radio interferometer through the relation [5, 6]

$$\delta r/r \simeq 0.5(\Delta\nu/\nu)(1+z)^{-1/2}. \qquad (3)$$

In Fig. 2 we plot the 21-cm dark ages signal power spectrum, Eq. (A3), in several redshifts using CAMB [7] in the limit of sharp frequency bandwidth and with a bandwidth of $\Delta\nu = 0.1\,{\rm MHz}$ (resulting in damping above $l\sim10^3$) in the linear regime. The signal peaks at redshift $z\sim60$ where the deviation between the spin temperature and that of the CMB is maximal [6]. We see that for a given bandwidth, the signal is roughly within the same order of magnitude for most redshifts up to very small angular scales, corresponding to arcsecond resolutions.

In Fig. 3 we plot the 21-cm EoR signal power spectrum, assuming reionization is instantaneous and complete at $z=7$, using the approximations in Eqs. (A4) and (A5) for a bandwidth of 1 MHz. The damping scale is again approximately $l\sim10^3$ (as the redshift of reionization is an order of magnitude smaller), and the signal is roughly constant for small scales up to $\gtrsim 10^4$, corresponding to slightly better than arcminute resolutions.

In the next section we compare the 21-cm signal with the noise power spectrum estimation of radio interferometers, before heading on to discuss the reconstruction of

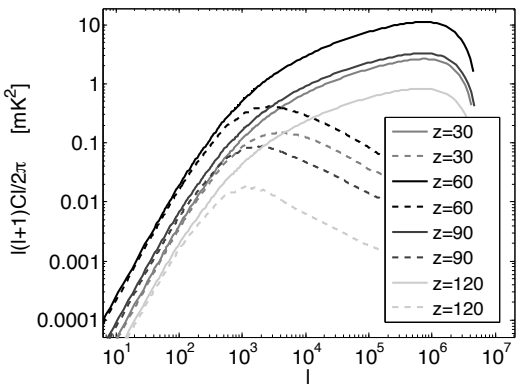

FIG. 2: 21-cm power spectrum for different redshifts during the dark ages, calculated using CAMB Sources [7]. Solid lines are calculated in the narrow-bandwidth limit and the signal is damped by the effect of baryon pressure at $l \gtrsim 10^6$. Dashed lines are for $\Delta\nu = 0.1\,\mathrm{MHz}$, where the signal is damped due to line-of-sight averaging over the bandwidth above $l \gtrsim 10^3$ as predicted by Eq. (3) for these redshift ranges.

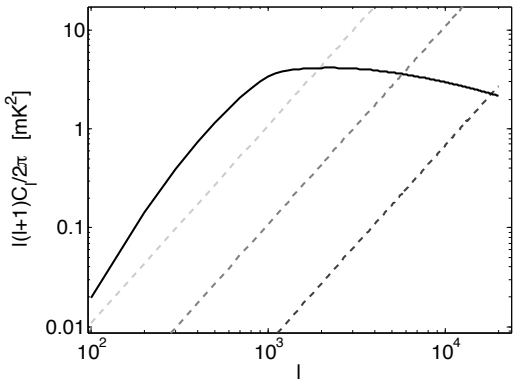

FIG. 3: 21-cm EoR power spectrum at redshift $z=7$, assuming complete and instantaneous reionization just after $z=7$, using Eqs. (A4) and (A5) (with an amplitude $\delta\bar{T}_b(\nu) \sim 20\,\mathrm{mK}$ [5]). The solid line is the signal power spectrum for a bandwidth of $\Delta\nu = 1$ MHz, which is damped around $l \lesssim 10^3$ for this redshift according to Eq. (3). Dashed lines are noise power spectra for SKA (light gray), SKA with $10\times t_0$ (medium gray) and SKA with $10 \times t_0$ and $4 \times f_{\mathrm{cover}}$ (dark gray). We see that with the final setup we can reach the maximum l observable with SKA's baseline of 6 km which is roughly $l_{\mathrm{cover}} \sim 2 \times 10^4$.

galaxy clusters from the weak lensing signal of the 21-cm radiation.

III. EXPERIMENTAL PROSPECTS

Following Ref. [5], we examine the noise power spectrum of a radio interferometer array. We denote by $l_{\mathrm{cover}}(\nu) = 2\pi D/\lambda$ the maximum mode at frequency ν (corresponding to wavelength λ) that can be measured with an array of dishes with maximum baseline D covering a total area A_{total} with a covering fraction $f_{\mathrm{cover}} \equiv N_{\mathrm{dish}} A_{\mathrm{dish}}/A_{\mathrm{total}}$. For uniform Fourier area coverage, a system temperature T_{sys}, a frequency window $\Delta\nu$, and an observing time t_o, the noise power spectrum is

$$l^2 C_l^n = \frac{(2\pi)^3 T_{\mathrm{sys}}^2(\nu)}{\Delta\nu t_o f_{\mathrm{cover}}^2} \left(\frac{l}{l_{\mathrm{cover}}(\nu)}\right)^2. \qquad (4)$$

Thus, for uniform Fourier coverage in an experiment targeting a frequency ν with bandwidth $\Delta\nu$, we conclude that $C_l^n \sim \mathrm{const} \equiv 2\pi\beta(\nu)(f_{\mathrm{cover}}^2\, t_0 \Delta\nu)^{-1}$, where $\beta(\nu) = (2\pi)^2 T_{\mathrm{sys}}^2(\nu)[l_{\mathrm{cover}}(\nu)^2]^{-1}$. As we can see from Figs. 2 and 3, on the relevant (small) scales for cluster reconstruction, the 21-cm radiation power spectrum at a given frequency and bandwidth behaves roughly (up to an order of magnitude) as $l^2 C_l \sim \mathrm{const} \equiv 2\pi\alpha(\nu, \Delta\nu)$. To find the value l_{max} beyond which the noise C_l^n is no longer negligible, we compare $C_{l_{\mathrm{max}}} = C_{l_{\mathrm{max}}}^n$ to find

$$l_{\mathrm{max}}^2 = \frac{\alpha(\nu, \Delta\nu)}{\beta(\nu)} (f_{\mathrm{cover}}^2\, t_0 \Delta\nu). \qquad (5)$$

This quantity depends trivially on the fractional coverage and observation time (they only affect the noise). The dependence on frequency and bandwidth is more elaborate, as we discuss later on below.

Observing the 21-cm anisotropies during the dark ages will be very challenging. The redshift range $30 < z < 200$ of absorption of the CMB at 21-cm ($\nu = 1420\,\mathrm{MHz}$) in the rest frame of the neutral-hydrogen gas corresponds to very low frequencies $7\,\mathrm{MHz} < \nu < 46\,\mathrm{MHz}$, where the sky temperature (dominated by foreground sources of synchrotron emission from the galaxy and from extragalactic sources) in regions of minimum emission at high galactic latitudes, approximately given by $T_{\mathrm{sys}} \sim 180\,(\nu/180\,\mathrm{MHz})^{-2.6}$ K, reaches $\sim 10^4 - 10^6$ K, many orders of magnitude above the signal $\sim 1\,\mathrm{mK}$ (as seen in Figs. 2 and 3).

While both galactic and extragalactic emissions vary smoothly and could be possibly subtracted by taking observations at two closely spaced frequencies, the additional sources of interference are harder to overcome. Terrestrial radio frequency interference is abundant in this range and is not spectrally smooth. Another source of contamination is the ionosphere which causes phase distortions in the cosmic signal and turns opaque at frequencies $\nu \lesssim 20\,\mathrm{MHz}$ (corresponding to $z > 70$). A futuristic experiment, based on placing a dark ages observatory on the far side of the Moon (which has no permanent ionosphere and its far side is shielded from terrestrial radio interference) was suggested in Ref. [4]. With a baseline on the order of $\gtrsim 10 - 100\,\mathrm{km}$, angular resolutions corresponding to $l_{\mathrm{max}} \sim 10^4 - 10^5$ (for source redshifts $z = 30 - 300$) might be reached in such an experiment, compensating for covering fraction and system temperature with prolonged observation time. With sufficient frequency coverage, the huge volume of CMB absorption in neutral hydrogen during the dark ages, $30 \lesssim z \lesssim 200$,

can be used to beat down the noise (by combining redshift slices, as we describe in the next Section) and measure the mass profile parameters of galaxy clusters to high accuracy.

To reach a measurement within the decade, the best candidate is the currently planned next generation experiment to measure 21-cm emission from neutral hydrogen during the EoR, the *Square Kilometer Array*[1] (SKA). With a design based on an extended region of $D\sim 6$ km where $l_{\rm cover}(\nu)\sim 10^4$ for the relevant frequencies in the epoch of reionization and $f_{\rm cover}\sim 0.02$, SKA can reach an observing time of order $t_0\sim 1000\,$hrs in one season covering up to an area of $\sim 2\pi\,$sr in the sky.

In Fig. 3 we plot several noise power spectra matching the current plans for a three-season run of SKA measuring at a frequency corresponding to redshift $z=7$ with a bandwidth of 1 MHz, as well as scenarios with an order of magnitude larger observation time, and with four times the coverage fraction. With the current plan, the maximum scale observable with a signal to noise greater than one is only $O(l_{\rm max}\sim 10^3)$. To reach $l_{\rm max}\gtrsim 10^4$ will require a considerable increase in coverage fraction and/or observation time.

IV. LENSING OF 21-CM FLUCTUATIONS BY A GALAXY CLUSTER

We now review the distortion to the 21-cm fluctuations induced by weak gravitational lensing. We assume that the lensing distortion takes place over a relatively small region of the sky, as should occur for lensing by a galaxy cluster, so that we can work in the flat-sky limit, where the analytic expressions are simpler.

Let $I_0(\vec{\theta})$ be the 21-cm intensity at position $\vec{\theta}$ on the sky. Lensing will deflect photons from $\vec{\theta}$ by an amount $\delta\vec{\theta}(\vec{\theta})=\nabla\phi(\vec{\theta})$. Here, $\phi(\vec{\theta})$ is the projected potential, related to the convergence $\kappa(\vec{\theta})=\Sigma(\vec{\theta})/\Sigma_{\rm cr}$, by $\nabla^2\phi=2\kappa$, where $\Sigma(\vec{\theta})$ is the surface mass density of the intervening cluster, and $\Sigma_{\rm cr}^{-1}=4\pi G D_d D_{ds}/(c^2 D_s)$ is the critical surface mass density in terms of the observer-lens, lens-source, and observer-source angular-diameter distances D_d, D_{ds}, and D_s, respectively. The observed intensity is thus $I(\vec{\theta})=I_0(\vec{\theta}+\delta\vec{\theta})\simeq I_0(\vec{\theta})+\delta\vec{\theta}\cdot\nabla I_0(\vec{\theta})$.

We suppose that intensity is measured over some square patch of sky of solid angle Ω, decomposed into $N_{\rm pix}$ pixels at positions θ_i, for $i=1,2,\ldots,N_{\rm pix}$, surrounding the cluster. The intensity can then be written in terms of Fourier coefficients,

$$I_{\vec{l}}=\frac{\Omega}{N_{\rm pix}}\sum_{\vec{\theta}_i} e^{i\vec{l}\cdot\vec{\theta}_i} I(\vec{\theta}_i), \tag{6}$$

as

$$I(\vec{\theta}_i)=\frac{1}{\Omega}\sum_{\vec{l}} e^{-i\vec{l}\cdot\vec{\theta}} I_{\vec{l}}, \tag{7}$$

where the sum is over the $N_{\rm pix}$ Fourier modes $\vec{l}$. The two-point intensity correlations are described by a power spectrum C_l defined by

$$\left\langle I_{\vec{l}} I^*_{\vec{l}'}\right\rangle=\Omega C_l\delta_{\vec{l},\vec{l}'} \tag{8}$$

The Fourier coefficients for the observed intensity are related to those of the unlensed intensity and deflection field by

$$I_{\vec{l}}=I_{0\vec{l}}-\frac{1}{\Omega}\sum_{\vec{l}'}\vec{l}'\cdot(\vec{l}-\vec{l}')\phi_{\vec{l}'}I_{0\,\vec{l}-\vec{l}'}, \tag{9}$$

from which it follows that for a fixed deflection field, the observed intensity satisfies

$$\left\langle I_{\vec{l}_1} I_{\vec{l}_2}\right\rangle=\Omega C_{l_1}\delta_{\vec{l}_1,-\vec{l}_2}+\phi_{\vec{L}}\vec{L}\cdot(\vec{l}_1 C_{l_1}+\vec{l}_2 C_{l_2}), \tag{10}$$

where $\vec{L}=\vec{l}_1+\vec{l}_2$ and the ensemble average is for a fixed deflection field.

Since $\kappa_{\vec{L}}=-L^2\phi_{\vec{L}}/2$, each $\vec{l}_1$-$\vec{l}_2$ pair of measured intensity Fourier modes with wavevectors $l_1+l_2=\vec{L}$ provides an estimator,

$$\widehat{\kappa^{\vec{l}_1,\vec{l}_2}_{\vec{L}}}=-\frac{L^2}{2}\frac{I_{\vec{l}_1}I_{\vec{l}_2}}{\vec{L}\cdot(\vec{l}_1 C_{l_1}+\vec{l}_2 C_{l_2})}, \tag{11}$$

and the variance of this estimator is

$$\left\langle\left(\widehat{\kappa^{\vec{l}_1,\vec{l}_2}_{\vec{L}}}\right)^2\right\rangle=\frac{L^4}{4}\frac{C^{\rm map}_{l_1}C^{\rm map}_{l_2}\Omega^2}{\left[\vec{L}\cdot(\vec{l}_1 C_{l_1}+\vec{l}_2 C_{l_2})\right]^2}, \tag{12}$$

where $C^{\rm map}_l=C_l+C^{\rm n}_l$ is the power spectrum of the intensity map, including the noise $C^{\rm n}_l$.

We can then sum the estimators $\widehat{\kappa^{\vec{l}_1,\vec{l}_2}_{\vec{L}}}$ over all $\vec{l}_1+\vec{l}_2=\vec{L}$ pairs (correcting for double counting of triangles with $\vec{l}\leftrightarrow\vec{L}-\vec{l}$) with inverse-variance weighting to obtain the minimum-variance estimator,

$$\begin{aligned}\widehat{\kappa_{\vec{L}}} \;=\; & -\frac{\Omega N_{\vec{L}}}{L^2}\sum_{\vec{l}}\frac{I_{\vec{l}}I_{\vec{L}-\vec{l}}}{\vec{L}\cdot(\vec{l}C_l+(\vec{L}-\vec{l})C_{|\vec{L}-\vec{l}|})} \\ & \times\left[\frac{C^{\rm map}_l C^{\rm map}_{|\vec{L}-\vec{l}|}\Omega^2}{[\vec{L}\cdot(\vec{l}C_l+(\vec{L}-\vec{l})C_{|\vec{L}-\vec{l}|})]^2}\right]^{-1},\end{aligned} \tag{13}$$

and

$$N^{-1}_{\vec{L}}=\frac{2\Omega}{L^4}\sum_{\vec{l}}\frac{[\vec{L}\cdot(\vec{l}C_l+(\vec{L}-\vec{l})C_{|\vec{L}-\vec{l}|})]^2}{C^{\rm map}_l C^{\rm map}_{|\vec{L}-\vec{l}|}\Omega^2} \tag{14}$$

[1] http://www.skatelescope.org

is the noise power spectrum for $\kappa_{\vec{L}}$. Equivalently, $\langle|\widehat{\kappa_{\vec{L}}}|^2\rangle = (2\pi)^2\delta(0)N_{\vec{L}} = \Omega N_{\vec{L}}$ is the variance with which $\kappa_{\vec{L}}$ can be measured.

We now use the continuum limit $\Omega^{-1}\sum_{\vec{l}} \to \int d^2l/(2\pi)^2$ and employ the simplifying assumption, Eq. (5), that the noise is small, $C_l^{\rm n} \ll C_l$, so that $C_l^{\rm map} \simeq C_l$, up to some scale $l_{\rm max}$. Then, in the limit $L \ll l$ we approximate $|\vec{L}-\vec{l}| \simeq l - L\cos\phi$, where $\cos\phi \equiv \hat{L}\cdot\hat{l}$, and then to first order, $C_{|\vec{L}-\vec{l}|} \simeq C_l - L(\cos\phi)(\partial C_l/\partial l)$, which yields [8]

$$N_{\vec{L}}^{-1} \simeq \frac{4}{L^4}\int\frac{d^2l}{(2\pi)^2}\frac{\left[\vec{L}\cdot\vec{l}C_l + \vec{L}\cdot(\vec{L}-\vec{l})C_{|\vec{L}-\vec{l}|}\right]^2}{2\,C_l\,C_{|\vec{L}-\vec{l}|}} \simeq \frac{l_{\rm max}^2}{2\pi}\left[1+\frac{\partial\ln C_l}{\partial\ln l}+\frac{3}{8}\left(\frac{\partial\ln C_l}{\partial\ln l}\right)^2\right]. \quad (15)$$

Using the approximation leading to Eq. (5), that the the noise for a single slice in an experiment at frequency ν with bandwidth $\Delta\nu$, a maximum baseline corresponding to $l_{\rm cover}$, a coverage fraction $f_{\rm cover}$, and observation time t_0, is approximately,

$$N_{\vec{L}} \sim \frac{4\pi}{l_{\rm max}^2} = \frac{4\pi\beta(\nu)}{\alpha(\nu,\Delta\nu)(f_{\rm cover}^2\,t_0\Delta\nu)}. \quad (16)$$

We can increase our signal considerably by changing the frequency at which the 21-cm map is made and thereby focus on spherical shells of neutral hydrogen at different redshifts. The above results for a single redshift slice can be extended to make use of the full redshift volume [8] by discretizing the z direction into radial components so that $C_{l,k}$ is the power in a mode with angular component l and radial components $k = 2\pi j/R$, where R is the total radial length of the volume. Under the assumption that modes with different k are independent, a total-volume estimator is built by summing the individual estimators, and the corresponding noise variance is

$$\frac{L^4/4}{N_{\vec{L}}} = \sum_k\int\frac{d^2l}{(2\pi)^2}\frac{[\vec{L}\cdot\vec{l}C_{l,k}+\vec{L}\cdot(\vec{L}-\vec{l})C_{|\vec{L}-\vec{l}|,k}]^2}{2C_{l,k}^{\rm map}C_{|\vec{L}-\vec{l}|,k}^{\rm map}} \quad (17)$$

In general, to estimate the number of slices available, we can think of 21-cm maps at two different frequencies that correspond to spherical shells separated along the line of sight by a comoving distance Δr. These will be statistically independent at the highest l provided that $(\Delta r/r_\nu) \gtrsim l^{-1}$. An experiment that covers a spatial range δr or a frequency range $\nu_1-\nu_2$ around a frequency ν will yield a total number of $N_z \sim (\delta r/\Delta r) \simeq l(\delta r/r_\nu) \simeq 0.5l((\nu_1-\nu_2)/\nu)(1+z)^{-1/2}$ statistically independent maps, which is roughly $N_z \sim 1500$ for the frequencies corresponding to the EoR at the maximum resolution of SKA and up to $N_z \sim 5000$ for a dark ages observatory with a baseline of 100 km (here we neglect the fact that different frequency bins are also somewhat correlated by contaminations). In practice, however, the tradeoff is a complicated one. While the signal is larger for narrow bandwidths, we saw in the last Section that the noise power spectrum around a given frequency increases as the frequency bandwidth is decreased, which limits the actual number of slices that can be combined in Eq. (17).

V. ESTIMATING CLUSTER PROPERTIES

Applying the estimator in Eq. (14) for the convergence $\widehat{\kappa}_L$ to a patch of sky around a galaxy cluster (assuming we know the location of its center to enough accuracy, say from other sources such as SZ surveys), we can retrieve a 2D image of the weak-lensing convergence of the cluster which we can study versus theory or simulation. The total number of pixels in Fourier space is the same as in real space. We then denote the N Fourier wavenumbers as $\vec{L}_i$ for $i = 1, 2, \ldots, N$. If $\widehat{\kappa_{\vec{L}_i}}$ is the measured value for the pixel i with variance $\langle|\widehat{\kappa_{\vec{L}_i}}|^2\rangle = \Omega N_{\vec{L}_i}$ and the corresponding theoretical value is $\kappa_{\vec{L}_i}^{\rm th}(M_{\rm fid})$ (calculated for some fiducial value $M_{\rm fid}$), then an estimator for the halo mass per pixel is given by

$$\widehat{M}_i = \frac{\widehat{\kappa_{\vec{L}_i}}}{\kappa_{\vec{L}_i}^{\rm th}(M_{\rm fid})}M_{\rm fid}, \quad (18)$$

with variance

$$\langle|\widehat{M}_i|^2\rangle = \frac{\Omega N_{\vec{L}_i}}{|\kappa_{\vec{L}_i}^{\rm th}(M_{\rm fid})|^2}M_{\rm fid}^2. \quad (19)$$

From these we can build a minimum-variance estimator,

$$\widehat{M} = \frac{\sum_i \widehat{M}_i/\langle|\widehat{M}_i|^2\rangle}{\sum_i 1/\langle|\widehat{M}_i|^2\rangle}, \quad (20)$$

for the mass as a weighted sum over the pixels. The variance of this estimator is, under the null hypothesis,

$$\sigma_M^{-2} = \sum_i 1/\langle|\widehat{M}_i|^2\rangle = \sum_{\vec{L}}\frac{|\kappa_{\vec{L}}^{\rm th}(M_{\rm fid})|^2}{M_{\rm fid}^2\Omega N_{\vec{L}}} \simeq \frac{N_z l_{\rm max}^2}{M_{\rm fid}^2\Omega 4\pi}\sum_{\vec{L}}|\kappa_{\vec{L}}^{\rm th}(M_{\rm fid})|^2|W_{\vec{L}}|^2 \simeq \frac{N_z l_{\rm max}^2}{M_{\rm fid}^2 4\pi}\int\frac{d^2\vec{L}}{(2\pi)^2}|\kappa_{\vec{L}}^{\rm th}(M_{\rm fid})W_{\vec{L}}|^2 = \frac{N_z l_{\rm max}^2}{M_{\rm fid}^2 4\pi}\int d^2\theta\left[\int d^2\varphi\, W(\vec{\varphi})\kappa(|\vec{\theta}-\vec{\varphi}|)\right]^2, \quad (21)$$

where in the second line we substituted

$$N_{\vec{L}} = \frac{4\pi}{N_z l_{\rm max}^2}e^{L^2/2L_{\rm max}^2} \equiv \frac{4\pi}{N_z l_{\rm max}^2}W_{\vec{L}}^{-1}, \quad (22)$$

with the exponential included to describe roughly the transition between those L modes that can be measured and those that cannot. In the third line in Eq. (21) we took the continuum limit $\sum_{\vec{L}} \Leftrightarrow \Omega \int d^2\vec{L}/(2\pi)^2$, and in the fourth we used Parseval's theorem to switch to real space, resulting in a convolution of the convergence with a two-dimensional Gaussian filter,

$$W(\varphi) = \frac{1}{2\pi\theta_s^2} e^{-\frac{\varphi^2}{2\theta_s^2}}, \tag{23}$$

with smoothing scale θ_s given by $\theta_s = \pi/L_{\rm max}$ (we assume here that we can push $L_{\rm max}$ close to $l_{\rm max}$ which is verified numerically). Assuming a spherically symmetric profile and cutting off the integral at Λ when the signal becomes negligible, we get

$$\sigma_M^{-2} = \frac{N_z l_{\rm max}^2}{2M_{\rm fid}^2} \int^{\Lambda} \theta\, d\theta \times \left[\int^{\Lambda} \varphi\, d\varphi\, W(\varphi) \int_0^{2\pi} d\phi\, \kappa(\sqrt{\theta^2+\varphi^2+2\theta\varphi\cos\phi}) \right]^2 . \tag{24}$$

This equation, together with Eq. (5), allows a straightforward examination of the capabilities of different telescopes to reconstruct a given lensing source. The focus of this work is detection of a galaxy cluster, but a similar formula can be used to estimate the signal-to-noise for reconstruction of model parameters for other lensing sources, as we discuss in the Conclusion.

The remaining task is to calculate the convergence profile of a given cluster. We model the mass profile of the galaxy cluster by an NFW profile [24],

$$\rho(r) = \rho_s \frac{1}{r/r_s(1+r/r_s)^2}, \tag{25}$$

where the scale radius r_s and normalization ρ_s are often described by the concentration parameter $c \equiv r_{\rm vir}/r_s$ and the cluster mass $M \equiv 4\pi r_s^3 \rho_s [\ln(1+c) - c/(1+c)]$. Here, $r_{\rm vir}$ is the radius within which the enclosed mass M is 200 times the average mass of the same volume in a critical density universe.

The convergence $\kappa(\theta)$ of the NFW profile is given by

$$\kappa(\theta = r/D_L) = \frac{2\rho_{\rm s} r_{\rm s}}{\Sigma_{\rm cr}} f(\theta/(r_s/D_L)), \tag{26}$$

where the functional form of the projected mass density is

$$f(x) = \begin{cases} \frac{1}{x^2-1}\left[1 - \frac{2}{\sqrt{x^2-1}} \arctan\sqrt{\frac{x-1}{x+1}}\right], & x > 1, \\ \frac{1}{3}, & x = 1, \\ \frac{1}{x^2-1}\left[1 - \frac{2}{\sqrt{1-x^2}} \operatorname{arctanh}\sqrt{\frac{1-x}{1+x}}\right], & x < 1. \end{cases} \tag{27}$$

In Fig. 4 we plot the convergence of a cluster at redshift $z = 1$ with mass of $M_1 = 5 \times 10^{14} h^{-1} M_\odot$ and concentration parameter $c = 3$ for a source at redshift $z = 7$. Plugging this in the integral of Eq. (24), we find that the signal-to-noise is saturated at the virial radius, so that effectively $\Lambda = r_{\rm vir}$, an order of magnitude above the corresponding Einstein radius. We also find that the dependence on the concentration parameter is small.

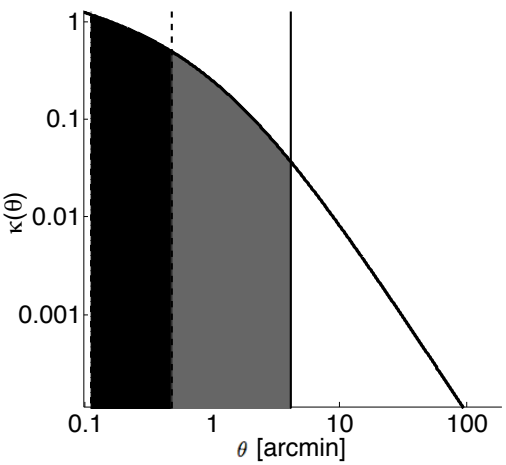

FIG. 4: The radial convergence of NFW clusters with mass of $M = 5 \times 10^{14} h^{-1} M_\odot$ and concentration $c = 3$ located at redshift $z = 1$, where the 21-cm source is at redshift $z = 7$. The vertical line marks the virial radii of the clusters where the signal becomes negligible. The two shaded regions show the amount of signal integrated with the ideal resolutions of SKA (*light shade*) at 1 arcmin and a dark ages observatory (*dark shade*) with a 100 km baseline at ~ 6 arcsec.

VI. RESULTS

To estimate the signal-to-noise with which this cluster mass can be reconstructed using the weak-lensing signal of 21-cm radiation measured by a radio interferometer, we consider the expected signal from the EoR from SKA (as described in the previous Section), an upgraded SKA with four times the collecting area, both with a bandwidth of 1 MHz, and an ideal experiment (capable of sustaining $C_l^s > C_l^n$ up to $l_{\rm max} = l_{\rm cover}$) with the same resolution as SKA ($l_{\rm cover} \gtrsim 10^4$) with a bandwidth small enough to reach the maximum number of independent redshift slices. We also include extremely optimistic limits for an ideal dark ages observatory with a baseline of 100 km (for which $l_{\rm cover} \sim 10^5$).

In Fig. 5 we plot the smallest detectable mass as a function of redshift, for different experimental capabilities. We see that with the current plans for SKA, the weak-lensing reconstruction of clusters as considered in Fig. 4 is completely beyond reach, unless about an order of magnitude more observation time is dedicated to the patch containing the target galaxy-cluster. Future experiments will narrow this gap and enable the mass measurement of significantly smaller mass halos using 21-cm

weak lensing.

These detection prospects involve intricate tradeoffs between the different experimental parameters. For example, if we increase observation time by 2, we can reach the same $l_{\rm max}$ with half the frequency bandwidth, which will also allow us to use twice the number of z-slices, increasing the S/N by $\sqrt{2}$. Alternatively, we could use this to reach a larger $l_{\rm max}$ (paying a small price for the damping in the signal power spectrum), which also increases the S/N, but this will still be limited by the maximum l set by the baseline of the interferometer. As mentioned in Section IV, one does not always do better by splitting up into smaller bandwidth bins because this increases the noise, yielding a smaller $l_{\rm max}$, which reduces the S/N and might also leave galaxy-cluster scales beyond reach. In addition, as we also discussed in Section IV, there is a lower limit to the frequency bandwidth (which determines the width of the redshift slices) below which the slices become correlated.

Another experimental issue is that as the observed frequency is increased in order to use multiple redshift slices, a larger baseline is needed to cover the same scales. This means that for a given experimental baseline, the contribution of additional slices degrades with their redshift and the S/N grows slower than $1/\sqrt{N_z}$. On the other hand, for high redshift clusters (which approach the sources of the EoR) the increase in lensing signal due to the larger line-of-sight distance traveled is larger than the loss in resolution, and so the S/N grows faster than $1/\sqrt{N_z}$.

To demonstrate this last point quantitatively[2], we plot in Fig. (6) the 1σ detection limits for two cluster redshifts as the number of redshift slices accumulated beyond $z=7$ is increased. We assume a bandwidth of $\Delta\nu = 0.1\,$MHz (yielding roughly ~ 800 slices in the range $z = 7 - 13$) and unlimited observation time so that the maximum resolution of SKA is reached. We see that the low redshift cluster gains less improvement in S/N as the number of redshifts is increased, because the smallest observable scale with a given baseline decreases with redshift. We also see that for a high redshift cluster, which is closer to the redshifts of the EoR, the benefit from the inclusion of additional redshift slices more than compensates for this degradation in resolution.

Finally, our estimator, Eq. 20, can be generalized to include the free parameters of the cluster location, which in this work we assumed were already known from other surveys.

[2] A full treatment must also take into account the redshift dependence of the 21-cm signal amplitude, which is not trivial, as can be seen for the dark ages in Fig. 2, but we neglect this for the purpose of this demonstration.

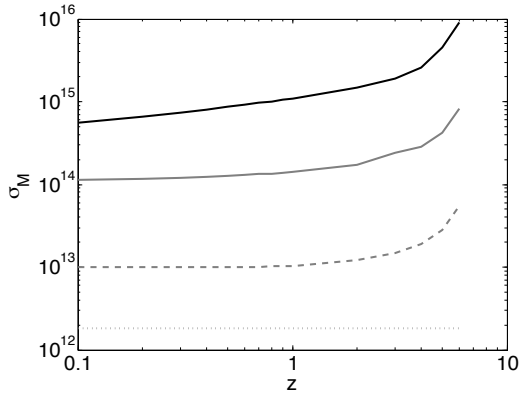

FIG. 5: The 1σ limit for weak lensing reconstruction for clusters in different redshifts up to the end of reionization ($z \sim 7$) using SKA (*thick solid line*), SKA with four times the coverage fraction or sixteen times the observing time (*thin solid line*), both with a bandwidth of 1 MHz, and for an ideal experiment with SKA resolution (*dashed line*). We also plot the expected limits for an ideal dark ages observatory with a 100 km baseline (*dotted line*).

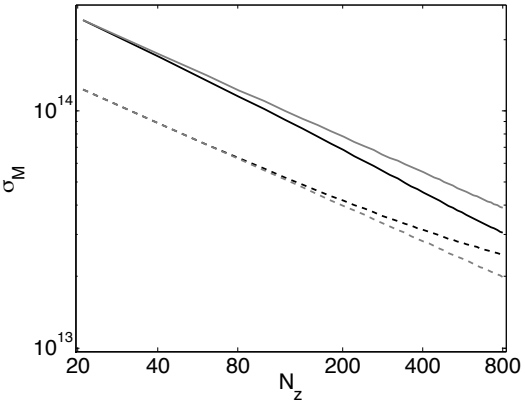

FIG. 6: The 1σ limit for weak lensing reconstruction for clusters at two redshifts, $z=0.5$ (*dashed black*) and $z=5$ (*solid black*), as we include more and more redshift slices beyond the end of reionization ($z \sim 7$), for SKA with frequency bandwidth $\Delta\nu = 0.1$MHz) and unlimited observation time. This takes into account the non-trivial source redshift dependence of the different slices. The gray lines are the results under the approximation of a trivial $1/\sqrt{N_z}$ dependence.

VII. DISCUSSION

We have constructed a minimum-variance estimator for the mass of a galaxy cluster using the weak-lensing convergence reconstruction of 21-cm fluctuations from the dark ages and the EoR. As has been suggested for CMB lensing reconstruction, possible improvements to the results shown here can stem from using modified weak-lensing estimators, enhancing sensitivity to small scales as in Ref. [25] or iteratively approaching a maximum-likelihood estimator as in Ref. [26]. Another option which has been discussed for CMB measurements

(e.g. Refs. [17, 25, 26]) is to stack reconstructed images of N different clusters to yield a $\sqrt{N}$ improvement in the signal-to-noise for fitting an overall mass profile (much like the use of different 21-cm redshift slices of the same cluster in Eq. (17)).

In comparison to other sources for weak-lensing measurements, such as galaxy shapes [27, 28], or CMB fluctuations [15] (detected recently [29]), the potential in 21-cm measurements is far greater. Even deep galaxy surveys will be limited to lower redshifts with small sky coverage and will not exceed arcminute resolutions. CMB lensing reconstruction at small scales is difficult because of the absence of power due to Silk damping at these scales and due to the ambiguity caused by the presence of a similar signature from the kinetic Sunyaev-Zeldovich effect on the CMB photons passing through the moving clusters [17, 26]. Even with ideal experiments at arcminute resolutions, the corresponding minimum galaxy-cluster mass detectable according to Eq. (24) with a CMB experiment is $M \sim 10^{15} h^{-1} M_\odot$. An average mass profile of $M \sim 10^{14} h^{-1} M_\odot$ can be measured with reasonable signal to noise by stacking thousands of galaxies, but the detailed reconstruction of an individual cluster is beyond the reach of these alternative methods.

Finally, an issue which we have neglected in this work is the influence of non-gaussianities which would have to be taken into account to yield accurate predictions. Particularly important is the effect of nonlinear structure [12, 30], which is relevant during the epoch of reionization, when certain patches of the IGM become substantially ionized well before its end. In order to properly account for these effects, the details of the reionization process will have to be uncovered. However, under the assumption that these features appear in higher resolutions than that of our considered interferometers [8, 10], there will be no connected four-point function contribution to the variance of the quadratic lensing estimator used here, and this treatment remains valid.

VIII. CONCLUSION

When 21-cm fluctuations become accessible to observations at small angular scales, the application of weak-lensing reconstruction methods will open the door to unprecedented precision measurements of local structure. We have found here that galaxy clusters can be detected by lensing reconstruction with futuristic experiments measuring CMB absorption by neutral hydrogen during the dark ages $30 \lesssim z \lesssim 200$ down to halo masses of order $M \gtrsim 10^{12} h^{-1}\, M_\odot$. Next-generation interferometers measuring emission from hot neutral-hydrogen gas during the epoch of reionization $7 \lesssim z \lesssim 13$ will be limited to $M \gtrsim 10^{15}\, h^{-1}\, M_\odot$ with the currently planned specifications. If, however, the collecting area or the observation time can be increased, they may be able to push the limit down to $M \gtrsim 10^{13}\, h^{-1}\, M_\odot$ (in particular, this can be reached by increasing the observation time dedicated to the target patch alone by two orders of magnitude). While these are challenging goals that remain unattainable in the near future, the potential achievements discussed here provide more motivation to invest in alleviating the experimental limitations.

Meanwhile, we can use the prescription described here to construct estimators for model parameters of other structures, from standard isothermal spheres and voids to more exotic structures such as cosmic textures [31, 32] or overdensities created by pre-inflationary particles [33, 34]. In future work we shall address the weak-lensing detectability, with 21-cm weak lensing, of voids or textures that might be responsible for the cold spot in WMAP CMB data [35, 36].

Acknowledgments

We thank the anonymous referee for excellent comments and suggestions which helped improve the quality of this paper. EDK was supported by the National Science Foundation under Grant Number PHY-0969020 and by the Texas Cosmology Center. This work was supported at Johns Hopkins by DoE SC-0008108 and NASA NNX12AE86G. EDK would like to thank the hospitality of the Department of Physics and Astronomy at Johns Hopkins, where this work was partially carried out.

Appendix A: Power spectrum of 21-cm fluctuations

We review the angular power spectrum of intensity fluctuations in the 21-cm signal induced by large-scale density inhomogeneities during the dark ages and the EoR, when redshift distortions are neglected. Following Refs. [1, 5], we start in three dimensions and first define the dimensionless fractional perturbation $\delta_{HI}(\mathbf{x}) \equiv [\delta T_b(\mathbf{x}) - \delta\bar{T}_b]/\delta\bar{T}_b$ of the brightness temperature (where $\delta\bar{T}_b$ is its mean), whose power spectrum in Fourier space is given by $\langle \delta_{HI}(\mathbf{k}_1)\, \delta_{HI}(\mathbf{k}_2)\rangle \equiv (2\pi)^3 \delta^3(\mathbf{k}_1 + \mathbf{k}_2) P(k_1, z)$ with its dimensionless counterpart $\Delta^2(k,z) = (k^3/2\pi^2) P(k,z)$. We move to two dimensions by integrating along the line of sight,

$$\delta_{HI}(\hat{\mathbf{n}}, \nu) = \int \mathrm{d}r\, W(r, r_\nu)\, \delta_{HI}(\hat{\mathbf{n}}, r), \qquad \text{(A1)}$$

with a projection window function $W(r, r_\nu)$ that peaks at the radial distance r_ν to the desired frequency ν within a width δr corresponding to an observational bandwidth $\Delta\nu$. To expand the brightness temperature in spherical harmonics, we use the planar wave expansion $e^{i\mathbf{k}\cdot\mathbf{x}} = \sum_{lm} 4\pi i^l j_l(kr) Y^*_{lm}(\hat{\mathbf{k}}) Y_{lm}(\hat{\mathbf{n}})$ (where $j_l(x)$ is the spherical Bessel function of order l), and

$$\begin{aligned} a_{lm}(\nu) &= 4\pi i^l \int \frac{\mathrm{d}^3 k}{(2\pi)^3} \delta_{HI}(\mathbf{k}, \nu) \alpha_l(k, \nu) Y^*_{lm}(\hat{\mathbf{k}}) \\ \alpha_l(k, \nu) &= \delta\bar{T}_b(\nu) \int \mathrm{d}r\, W(r, r_\nu)\, j_l(kr)\ . \end{aligned} \qquad \text{(A2)}$$

The brightness temperature power spectrum of 21-cm fluctuations, defined as $\langle a_{lm}(\nu) a^*_{l'm'}(\nu')\rangle \equiv \delta_{ll'}\delta_{mm'} C_l(\nu,\nu')$, is then given by

$$C_l(\nu,\nu') = 4\pi \int \mathrm{d}k \frac{\Delta^2(k,z)}{k} \alpha_l(k,\nu)\alpha_l(k,\nu'). \quad \text{(A3)}$$

Under the approximation $\Delta^2(k,z) \approx \Delta^2(l/r_\nu, z)$, for a pure power-law power spectrum and for large angular scales $l\delta r/r \ll 1$, the line of sight integration is approximately a delta function and we get

$$\frac{l^2 C_l(\nu,\nu)}{2\pi} \propto \delta\bar{T}_b^2(\nu)\Delta^2(l/r_\nu, z). \quad \text{(A4)}$$

For the purposes of reconstructing galaxy-cluster profiles, we are mostly interested in the smallest observable scales, which satisfy the limit $l\delta r/r \gg 1$. Applying the Limber approximation [21, 22] in Fourier space [23] yields

$$\frac{l^2 C_l(\nu,\nu)}{2\pi} \propto \delta\bar{T}_b^2(\nu)\Delta^2(l/r_\nu, z)\frac{r_\nu}{l\,\delta r}, \quad \text{(A5)}$$

where we see the suppression of small-angle fluctuations resulting from averaging out of modes $k \gtrsim 1/\delta r$ in Eq. (A1).

[1] S. Furlanetto, S. P. Oh and F. Briggs, Phys. Rept. **433**, 181 (2006) [astro-ph/0608032].

[2] J. R. Pritchard and A. Loeb, Rept. Prog. Phys. **75**, 086901 (2012) [arXiv:1109.6012 [astro-ph.CO]].

[3] J. D. Bowman and A. E. E. Rogers, Nature **468**, 796 (2010); G. Paciga *et al.* (GMRT-EoR Collaboration), Mon. Not. R. Astron. Soc. **413**, 1174 (2011); `www.lofar.org`; `www.mwatelescope.org`; `web.phys.cmu.edu/ past`; `www.phys.unm.edu/ lwa`; `astro.berkeley.edu/ dbacker/eor`; `www.haystack.mit.edu/ast/arrays/Edges`; `www.skatelescope.org`.

[4] S. Jester and H. Falcke, New Astron. Rev. **53**, 1 (2009) [arXiv:0902.0493 [astro-ph.CO]]; T. J. W. Lazio, J. Burns, D. Jones, J. Kasper, S. Neff, R. MacDowall, K. Weiler, and DALI/ROLSS Team, Bulletin of the American Astronomical Society 41, 344 (2009); J. O. Burns, T. J. W. Lazio and W. Bottke, arXiv:1209.2233 [astro-ph.CO].

[5] M. Zaldarriaga, S. R. Furlanetto and L. Hernquist, Astrophys. J. **608**, 622 (2004) [astro-ph/0311514].

[6] A. Loeb and M. Zaldarriaga, Phys. Rev. Lett. **92**, 211301 (2004) [arXiv:astro-ph/0312134].

[7] A. Lewis and A. Challinor, Phys. Rev. D **76**, 083005 (2007) [astro-ph/0702600 [ASTRO-PH]].

[8] O. Zahn and M. Zaldarriaga, Astrophys. J. **653**, 922 (2006) [astro-ph/0511547].

[9] R. B. Metcalf and S. D. M. White, Mon. Not. Roy. Astron. Soc. **394**, 704 (2009) [arXiv:0801.2571 [astro-ph]].

[10] R. B. Metcalf and S. D. M. White, Mon. Not. Roy. Astron. Soc. **381**, 447 (2007) [arXiv:0611862 [astro-ph]].

[11] S. Hilbert, R. B. Metcalf and S. D. M. White, Mon. Not. Roy. Astron. Soc. **382**, 1494 (2007) [arXiv:0706.0849 [astro-ph]].

[12] T. Lu and U. -L. Pen, [arXiv:0710.1108 [astro-ph]].

[13] K. Sigurdson and A. Cooray, Phys. Rev. Lett. **95**, 211303 (2005) [astro-ph/0502549].

[14] L. Book, M. Kamionkowski and F. Schmidt, Phys. Rev. Lett. **108**, 211301 (2012) [arXiv:1112.0567 [astro-ph.CO]].

[15] M. Zaldarriaga, U. Seljak, Phys. Rev. **D59**, 123507 (1999) [astro-ph/9810257]; U. Seljak and M. Zaldarriaga, Phys. Rev. Lett. **82**, 2636 (1999) [astro-ph/9810092]; W. Hu, Phys. Rev. **D64**, 083005 (2001) [astro-ph/0105117]; Astrophys. J. **557**, L79 (2001) [astro-ph/0105424]; W. Hu and T. Okamoto, Astrophys. J. **574**, 566 (2002) [astro-ph/0111606]; M. H. Kesden, A. Cooray and M. Kamionkowski, Phys. Rev. **D67**, 123507 (2003) [astro-ph/0302536]; A. Lewis and A. Challinor, Phys. Rept. **429**, 1 (2006) [astro-ph/0601594]; S. Dodelson, F. Schmidt and A. Vallinotto, Phys. Rev. D **78**, 043508 (2008) [arXiv:0806.0331 [astro-ph]]; A. Cooray, M. Kamionkowski and R. R. Caldwell, Phys. Rev. D **71**, 123527 (2005) [astro-ph/0503002].

[16] T. Okamoto and W. Hu, Phys. Rev. D **67**, 083002 (2003) [astro-ph/0301031].

[17] W. Hu, S. DeDeo and C. Vale, New J. Phys. **9**, 441 (2007) [astro-ph/0701276].

[18] J. Silk, Astrophys. J. **151**, 459 (1968).

[19] A. Albrecht *et al.*, ArXiv Astrophysics e-prints (2006), [astro-ph/0609591].

[20] G. B. Field, Astrophys. J. **129**, 525 (1959).

[21] D. N. Limber, Astrophys. J. **117**, 134 (1953);

[22] P. J. E. Peebles, *The Large-Scale Structure of the Universe* (Princeton University Press, Princeton, 1980).

[23] N. Kaiser, Astrophys. J. **388**, 272 (1992).

[24] J. F. Navarro, C. S. Frenk and S. D. M. White, Astrophys. J. **490**, 493 (1997) [astro-ph/9611107].

[25] M. Maturi, M. Bartelmann, M. Meneghetti and L. Moscardini, Astron. Astrophys. **436**, 37 (2005) [astro-ph/0408064].

[26] J. Yoo and M. Zaldarriaga, Phys. Rev. D **78**, 083002 (2008) [arXiv:0805.2155 [astro-ph]].

[27] R. D. Blandford *et al.*, Mon. Not. Roy. Astron. Soc. **251**, 600 (1991); J. Miralda-Escudé, Astrophys. J. **380**, 1 (1991); N. Kaiser, Astrophys. J. **388**, 272 (1992); M. Bartelmann and P. Schneider, Astron. Astrophys. **259**, 413 (1992); M. Kamionkowski, A. Babul, C. M. Cress and A. Refregier, Mon. Not. Roy. Astron. Soc. **301**, 1064 (1998) [astro-ph/9712030]; M. Bartelmann and P. Schneider, Phys. Rept. **340**, 291 (2001) [astro-ph/9912508].

[28] D. J. Bacon, A. R. Refregier and R. S. Ellis, Mon. Not. Roy. Astron. Soc. **318**, 625 (2000) [astro-ph/0003008]; N. Kaiser, G. Wilson and G. A. Luppino, Astrophys. J. **556**, 601 (2001) [astro-ph/0003338]; D. M. Wittman *et al.*, Nature **405**, 143 (2000) [astro-ph/0003014]; L. van Waerbeke *et al.*, Astron. Astrophys. **358**, 30 (2000) [astro-ph/0002500].

[29] K. M. Smith, O. Zahn and O. Dore, Phys. Rev. D **76**, 043510 (2007) [arXiv:0705.3980 [astro-ph]]; C. M. Hirata

et al., Phys. Rev. D **78**, 043520 (2008) [arXiv:0801.0644 [astro-ph]]; S. Das *et al.* (ACT Collaboration), Phys. Rev. Lett. **107**, 021301 (2011) [arXiv:1103.2124 [astro-ph.CO]].
[30] T. Lu, U. -L. Pen and O. Dore, Phys. Rev. D **81**, 123015 (2010) [arXiv:0905.0499 [astro-ph.CO]].
[31] N. Turok, Phys. Rev. Lett. **63**, 2625 (1989).
[32] N. Turok and D. Spergel, Phys. Rev. Lett. **64**, 2736 (1990).
[33] A. Fialkov, N. Itzhaki and E. D. Kovetz, JCAP **1002**, 004 (2010) [arXiv:0911.2100 [astro-ph.CO]].
[34] B. Rathaus and N. Itzhaki, JCAP **1205**, 006 (2012) [arXiv:1202.5178 [astro-ph.CO]].
[35] S. Das and D. N. Spergel, Phys. Rev. D **79**, 043007 (2009) [arXiv:0809.4704 [astro-ph]].
[36] B. Rathaus, A. Fialkov and N. Itzhaki, JCAP **1106**, 033 (2011) [arXiv:1105.2940 [astro-ph.CO]].